Microbial Cell Factories

RESEARCH

Open Access

# High-efficiency production of plant-derived pigment dopaxanthin in *Escherichia coli* by combination engineering

Xiaolong Jiang[1,2†], Liyan Tian[1,2†], Wujiu Chen[1,2] and Qinhong Wang[1,2*]

## Abstract

**Background** Dopaxanthin is a natural pigment betaxanthins family member with the highest antioxidant and free radical scavenging activities. However, its relatively low content in plants limited the wide range of applications. Cost-efficient microbial production, therefore, showed an attractive alternative.

**Results** Here, an *Escherichia coli* strain equipped with the de novo biosynthetic pathway for hyperproducing dopaxanthin was constructed by combining metabolic engineering and protein engineering. Firstly, a high-performance rate-limiting levodopa 4,5-dioxygenase (DODA) was mined and characterized based on sequence similarity searching followed by whole-cell catalysis and de novo synthesis strategy. Then, the catalytic efficiency of DODA was increased 34 times with directed evolution. The mutated DODA significantly facilitated the production of dopaxanthin, with an increase of 40.17% in plasmid expression and 64.11% in genome expression, respectively. Finally, through connecting the blocked pathway from 3-dehydroshikimate to levodopa (L-DOPAOPA) and enhancing the expression level of DODA, a titer of dopaxanthin of 22.87 g/L was achieved from glucose as feedstock, which is 286 times higher than that in the previous report.

**Conclusion** This work not only established a promising platform for the environmentally friendly production of dopaxanthin but also laid a foundation for the commercialization of other betalain.

**Keywords** Dopaxanthin, High-performance, DODA, Directed evolution, De novo synthesis

## Introduction

Betalains are water-soluble N-heterocyclic hydrophilic pigments divided into yellow-orange betaxanthins and red-violet betacyanins [1]. They were mainly found in the *Caryophyllales* order of plants [2] and the higher fungi *Amanita* and *Hygrocybe* [3]. The most significant application of betalains is that they can be used as food colorants and dietary supplements under the E-162 code in the European Union [4] and as the additive 73.40 in the 21 CFR section of the Food and Drug Administration (FDA) in the United States [5].

Dopaxanthin is an essential molecule of betaxanthins, containing dihydroxyl groups that possess the highest antioxidant and free radical scavenging activities [6, 7]. It can be further converted into betanin, the core molecule of betacyanins, with several enzymes, including *O*-glycosyltransferase [8]. As a natural yellow-orange pigment, dopaxanthin provides another shade and bioactive constituent for the coloration and health benefits of foods and beverages [9, 10]. Dopaxanthin can be found in

†Xiaolong Jiang and Liyan Tian are contributed equally to this work.

*Correspondence:
Qinhong Wang
wang_qh@tib.cas.cn
[1] Key Laboratory of Engineering Biology for Low-carbon Manufacturing, Tianjin Institute of Industrial Biotechnology, Chinese Academy of Sciences, Tianjin 300308, China
[2] National Center of Technology Innovation for Synthetic Biology, Tianjin 300308, China

*Glottiphyllum* [11, 12], *Portulaca* [13], and *Lampranthus* [14]. However, its low content in plants hampers potential applications.

Recent discoveries led to the completion of the core betalain dopaxanthin biosynthetic pathway puzzle, paving the way from extraction to plant cell suspension cultures and microbial production. As illustrated in Fig. 1, dopaxanthin is derived from the tyrosine metabolism pathway, followed by 3-hydroxylated to form L-DOPAOPA, and L-DOPAOPA is subsequently

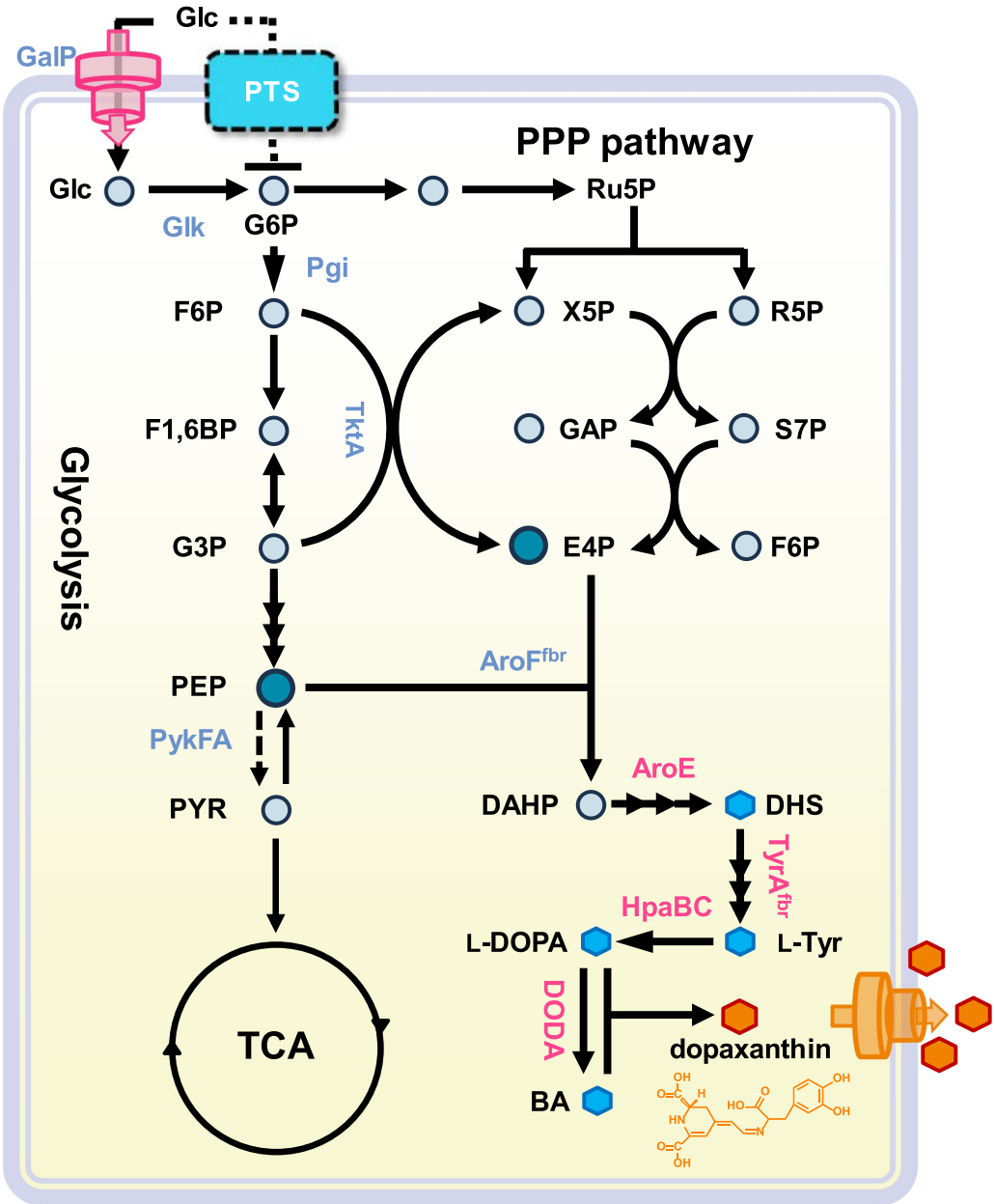


**Fig. 1** Schematic diagram of dopaxanthin production by Betalain-Platform *E. coli*. Abbreviation: Glc, glucose; G6P, D-glucose 6-phosphate; Ru5P, D-ribulose 5-phosphate; F6P, D-fructose 6-phosphate; X5P, D-xylulose 5-phosphate; R5P, D-ribose 5-phosphate; F1,6BP, D-fructose 1,6-bisphosphate; G3P, D-glycerate 3-phosphate; GAP, D-glyceraldehyde 3-phosphate; S7P, D-sedoheptulose 7-phosphate; PEP, phosphoenolpyruvate; E4P, D-erythrose 4-phosphate; PYR, pyruvate; DAHP, 3-deoxy-D-arabino-heptulosonic acid 7-phosphate; DHS, 3-dehydroshikimate; L-Tyr, L-tyrosine; L-DOPA, 3,4-dihydroxy-L-phenylalanine; BA, betalamic acid; PPP pathway, pentose phosphate pathway; TCA, citrate cycle; PTS, phosphotransferase system; GalP, galactose H(+) symporter; Glk, glucokinase; Pgi, glucose-6-phosphate isomerase; TktA, transketolase I; PykA, pyruvate kinase II; PykF, pyruvate kinase I; AroF$^{fbr}$, feedback relieved 3-deoxy-7-phosphoheptulonate synthase; AroE, shikimate dehydrogenase; TyrA$^{fbr}$, feedback relieved prephenate dehydrogenase; HpaB, 4-hydroxyphenylacetate 3-hydroxylase; HpaC, flavin reductase; DODA, DOPA-4,5-dioxygenase

oxidized to unstable 4,5-seco-DOPA by DODA. This compound is then non-enzymatically rearranged to betalamic acid, the core chromophore in all betalains. Betalamic acid spontaneously undergoes a Schiff-base condensation with L-DOPAOPA via its reactive aldehyde group to produce dopaxanthin. Several studies about the heterologous synthesis of dopaxanthin were reported recently. Cell cultures of *Celosia argentea* were developed to produce betaxanthins dopaxanthin and miraxanthin V and the betacyanins betanidin and decarboxy-betanidin with a relatively low titer after eight days of culture [10]. Hou and coauthors engineered *E. coli* to produce betaxanthin by overexpressing HpaBC and *Mj*DODA [15]. They obtained various betaxanthins and betacyanins, including dopaxanthin, by feeding different amino acids and amines to strain BTA6. Maria Alejandra Guerrero-Rubio and coauthors employed whole-cell catalysis to produce four different betaxanthins and two betacyanins, the titer reaching 79.96 mg/L for dopaxanthin, through supplementing L-DOPAOPA to betalamic acid-containing broth which was created by *Gd*DODA-containing *E. coli* [16]. Besides prokaryote *E. coli*, there also were many efforts to produce dopaxanthin in yeast. Dopaxanthin was produced in *Saccharomyces cerevisiae* through combinatorial assembly of twelve DODA variants and eleven tyrosine hydroxylase variants by implementing a highthroughput engineering method coupled with the fluorescence-activated cell sorting technique [17]. This method significantly enhanced the efficiency of enzyme combination screening, thereby allowing engineered yeast to in vivo produce high content of dopaxanthin, avoiding the common method of producing dopaxanthin in *E. coli*—the addition of precursors L-DOPA and amino acid.

None of reported studies about heterologous biosynthesis of betalain molecules addressed the low performance of the first key enzyme, DODA. Hence, it is urgent to elevate DODA performance through protein engineering. The titer of critical precursor L-DOPA, synthesized by engineered strains,was also low. Moreover, several reported strains even could not produce L-DOPA, which could only be replaced with a feeding strategy. These defects pushed up the cost of microbial synthesis of betalain and hindered its scientific and commercial application.

To achieve an L-DOPA-hyperproducing strain, several vital enzymes in the DHS-hyperproducing starting strain, including AroE, TyrA, and HpaBC, were up-regulated by the high-expression-level part. The strain thus constructed produced L-DOPA with the highest titer reported so far. To funnel the high content of precursor L-DOPA to dopaxanthin, an effective dioxygenase *Vv*DODA that was lacking in the de novo synthetic pathway of dopaxanthin was mined through sequence similarity searching, whole-cell catalysis and flask fermentation based on the reported DODAs. Subsequently, the *Vv*DODA was inserted into the genome of L-DOPA-hyperproducing strain with a high-expression-level part. The conceived strain produced a high titer of dopaxanthin, exceeding previous reports. Although a high concentration of dopaxanthin was obtained, the large amount of residual L-DOPA indicated the insufficient activity of the wild-type *Vv*DODA. Therefore, an effective protein evolution strategy was designed to improve the performance of *Vv*DODA. The catalytic efficiency of DODA was increased significantly with this strategy and the titer of dopaxanthin was dramatically enhanced by the facilitation of evolved DODA. Pocket prediction based on structural modeling showed that the improvement in catalytic efficiency was caused by the reduced volume of catalytic pockets and the increase of catalytic openings. Furthermore, the biosynthetic pathway was optimized to enhance the production efficiency of dopaxanthin. Finally, a promising platform strain was established, which could de novo produce 22.87 g/L natural pigment dopaxanthin with a yield 286 times higher than the previous report.

## Materials and methods

### Strains, plasmids, primer sets, and DNA manipulation methods

Tables S1-S4 showed strains, plasmids, primer sets, and nucleotide sequences included in this study. WJ060 (Table S1), which could produce 90 g/L 3-dehydroshikimate [18] was genetically modified to produce dopaxanthin. The pTLY series plasmids were propagated in DH5α using LB medium. The DODA sequences were codon-optimized and synthesized by Tsingke Biotech (Beijing, China). Plasmid pet30-$P_{M1\text{-}93}$ was achieved by inserting $P_{M1\text{-}93}$ sequence [19] between *Xba*I and *Bam*HI site of pet30a (+). All the accession numbers and corresponding sequences are listed in Table S4. To produce dopaxanthin, cassettes $P_{M1\text{-}93}$-*Vvdoda* and its mutants were seamlessly inserted into *ygiD*, *ldhA*, or *pflB* loci through Red-mediated homologous combination [20]. Successful mutants were verified by PCR and sequencing.

### Mining high-efficiency DODA

The phylogenetic tree of DODAs was constructed using MEGA-X software based on the protein sequence comparisons of *Am*DODA, *Mj*DODA, and *Bv*DODA homologs from different betalain-producing species. 25 sequences were selected based on no less than 45%

identity. Multiple sequence alignments were performed using the ClustalW program and processed to generate a maximum likelihood phylogenetic tree for molecular evolutionary analysis.

The pTLY1 to pTLY25 series plasmids, which were verified by sequencing, harboring the genes of different DODAs, were then introduced into BL21(DE3). A single colony was grown overnight in LB broth at 37 °C and 220 rpm. 1% overnight culture was inoculated into 50 mL LB broth with an $OD_{600}$ of 0.03–0.05 and grown at 37 °C and 220 rpm. When $OD_{600}$ reached 0.6, 1 mM IPTG was supplemented for the following 5–6 h induction at 30 °C and 220 rpm. Whole-cell catalysts were harvested through a centrifuge at 5000×*g* for 5 min. The catalysis reaction was carried for 12 h or 24 h in 10 mL PBS buffer (0.01 M, pH 6.0) containing 10 mM L-DOPA and 1.0 or 5.0 $OD_{600}$ whole-cell catalyst at 20, 30, or 37 °C. The supernatant of the catalysis mixture was subjected to dopaxanthin determination. Afterward, the DODAs that produce higher concentrations of dopaxanthin were further compared under the pH range from 6.0 to 7.5.

### Establishment of mutant library and high throughput screen

To improve the activity of *Vv*DODA, the mutant library of the *Vvdoda* gene was created by error-prone PCR. The PCR reaction volume is 50 μL, consisting of 1 μL EasyTaq® DNA Polymerase (Transgene, Beijing, China), 5 μL 10 × Buffer, 0.2 mM dNTPs, 3 mM $MgSO_4$, 0.4 mM $MnCl_2$, 0.2 μM sense and antisense primers, and 1 ng DNA template. The amplification reaction was carried out as follows: 94 °C for 3 min; 94 °C for 30 s, 55 °C for 30 s, 72 °C for 1 min, repeated 30 times; 72 °C for 5 min. The gel-purified fragments were ligated to *Bam*HI and *Hind*III-digested plasmid pet30a-$P_{M1\text{-}93}$ using NEBuilder® HiFi DNA Assembly Kit (NEB, USA) and then transformed into host strain TLYB1.

50 μL transformed TLYB1 was pooled and spread on an LB plate with 50 mg/L kanamycin. Seed culture was prepared by inoculating 96 single colonies into 96-well plates (LSYGEN, Tianjin, China) containing 500 μL of LB medium, with one single colony per well. The plate was incubated overnight at 37 °C and 800 rpm on an orbital shaker (ZQZY-88CV, Zhichu Instruments, China). Subsequently, 50 μL of the seed culture was transferred to a new 96-well plate containing 500 μL of NBS medium [18] in each well. The plate was further incubated at 37 °C and 800 rpm for 36 h. Afterward, 20 μL of the supernatant from each well was diluted with 180 μL of $ddH_2O$, and absorbance at 471 nm was measured with a multifunctional microplate reader (M2E, Molecular Devices, USA).

### Purification and characterization of *Vv*DODA, *Vv*DODA$^{I103V}$ and *Vv*DODA$^{I103V/R114A}$

The TLYA19, TLYA26, and TLYA27 with *Vv*DODA, *Vv*DODA$^{I103V}$, and *Vv*DODA$^{I103V/R114A}$, respectively, were inoculated into 50 mL LB medium with an $OD_{600}$ of 0.05. The cultures were grown at 37 °C and 220 rpm. When $OD_{600}$ reached 0.6–0.8, 1 mM IPTG was supplemented for subsequent 4 h induction at 30 °C. Bacteria were harvested, washed with 0.9% NaCl, suspended in binding buffer (30 mM Tris, 200 mM NaCl, pH 8.0), followed by homogenization with homogenizer JN-100C (JNBIO, Guangzhou, China) at 800 bar. Target proteins were purified by gravity-flow chromatography using a nickel-charged resin Ni–NTA Agarose (GenScript). The solubility and purity of the target protein are visualized through SDS-PAGE analysis. Protein concentrations were determined by the dye-binding method of the Bradford assay (Solarbio). Bovine serum albumin was used as the calibration standard.

The kinetic parameters of *Vv*DODA and each mutant protein to L-DOPA were determined at 37 °C by incubating 1.0 μM of the enzyme with a concentration range from 1.0 to 6.0 mM of L-DOPA in sodium phosphate buffer (50 mM, pH 7.0) with a spectrophotometer (Molecular Devices SpectraMax M2e, USA). The data was collected every 10 s for 5 min. Product formation was monitored by the increase in absorption at 414 nm over time, and the initial rate of product formation (μM/min) was calculated by linear regression, assuming the molar absorptivity coefficient (ε) at 424 nm to be 24,000/(M cm) for both products [21]. The specific activity at each substrate concentration was plotted. The value of Km and Vmax was fitted through a non-linear regression method using the Michaelis–Menten equation. The crude enzyme activity of TLYB7 and TLYB8 was determined by incubating 100 μL of the 10 $OD_{600}$ disrupted bacteria supernatant with 10 mM of L-DOPA in 1 mL volume. The supernatant of TLYB6 was used as a reference.

To determine the effect of pH and temperature on DODA activity, a 1 mL 50 mM sodium phosphate buffer mixture was prepared, the pH of the buffer was adjusted to 6.0, 6.2, 6.5, 6.7, 7.0, 7.2, 7.5, and 8.0, and the temperature was set to 20, 25, 30, 37, 40, 45, 50, 55 and 60 ℃. 10 mM L-DOPA and 1.0 μM protein were used in the reaction mixtures for 5 min.

### Fermentation conditions and metabolites assay

For flask fermentation, a single colony was inoculated into a 50-mL flask containing 20 mL LB medium

and incubated overnight at 37 °C and 800 rpm. The overnight culture was inoculated at a ratio of 1:50 into 10 mL NBS medium (20 g/L Glucose, 3.5 g/L $KH_2PO_4$, 6.5 g/L $K_2HPO_4{\cdot}3H_2O$, 3.5 g/L $(NH_4)_2HPO_4$, 0.25 g/L $MgSO_4{\cdot}7H_2O$, 15 mg/L $CaCl_2{\cdot}2H_2O$, 1.6 mg/L $FeCl_3{\cdot}6H_2O$, 0.2 mg/L $CoCl_2{\cdot}6H_2O$, 0.1 mg/L $CuCl_2{\cdot}2H_2O$, 0.2 mg/L $ZnCl_2$, 0.2 mg/L $Na_2MoO_4{\cdot}2H_2O$, 0.05 mg/L $H_3BO_3$). The fermentation lasted 36 or 48 h at 220 rpm and 37 °C. If necessary, 50 μg/mL of kanamycin was added.

Fed-batch fermentations were performed with a 5-L bioreactor (Biotech-5BG, Bxbio, China). A single colony was grown overnight in 20 mL LB medium at 220 rpm and 37 °C. Then, all the overnight culture was transferred to 180 mL LB medium for another 12 h of cultivation. The 200 mL seed culture was transferred to the 5-L bioreactor containing 1.8 L initial fermentation medium (7.5 g/L $K_2HPO_4{\cdot}3H_2O$, 2 g/L $MgSO_4{\cdot}7H_2O$, 1.6 g/L $(NH_4)_2SO_4$, 0.0756 g/L $FeSO_4{\cdot}7H_2O$, 2 g/L Citric acid, 4.525 mg/L $MnSO_4{\cdot}H_2O$, 20 mg/L $Na_2SO_4$, 6.4 mg/L $ZnSO_4$, 4 mg/L $CoCl_2{\cdot}6H_2O$, 0.6 mg/L $CuSO_4{\cdot}5H_2O$). The glucose (600 g/L) was fed to maintain the glucose concentration of fermentation broth at 0.1–5 g/L after the initial glucose (30 g/L) was exhausted. The pH was automatically maintained at 6.0 using 25% $NH_3{\cdot}H_2O$, and the fermentation temperature was maintained at 37 ℃. The stirring rate ranged from 300 to 950 rpm, and the ventilation rate was set at 1–2 vvm to maintain the dissolved oxygen level at 20% saturation. Samples were collected every 4 h to analyze dopaxanthin, glucose, and L-DOPA content in the fermentation broth.

An Agilent 1260 apparatus (CA, USA) with a DAD detector was used for calibration curve drawing and metabolite determination. 10 μL sample was loaded onto an Innoval C-18 column (250 × 4.6 mm, 5 μm, Agela tech, Tianjin, China) and separated by isocratic elution composed of 80% solvent A and 20% solvent B at UV 280, 414 and 471 nm. Solvent A comprised 99.9% distilled and deionized water with 0.1% phosphoric acid, and solvent B comprised 100% methanol. The flow rate was 0.8 mL/min, operated at 30 °C. The culture media were centrifuged for 10 min at 14,000×g, and the supernatants were analyzed.

#### Purification and characterization of dopaxanthin

For the MS analysis of dopaxanthin in fermentation broth, 10 μL of filtered supernatant was subjected to HPLC-HRMS analysis using an Agilent 1290 apparatus (CA, USA) equipped with an Innoval C-18 column (250 × 4.6 mm, 5 μm, Angela tech, China) and coupled to a Bruker Daltonics microTOF-QII mass spectrometer fitted with an electrospray source operated in positive mode. To accurately quantify the concentration in the fermentation and catalytic broth, we need to get authentic dopaxanthin. 20 mL supernatant from the 5-L scale-up fermentation broth of TLYB4 was injected into a preparative dynamic axial compression column, which was filled with pentafluorophenyl bonded silica gel (250 × 50 mm, 10 μm, Hanbon Sci and Tech, China). Elution was performed at UV 280 and 471 nm using a gradient of acetonitrile (solvent C) and 0.1% acetic acid aqueous (solvent D): 0–10 min, 100% solvent D; 10–35 min, 100%–90% solvent D; 35–40 min, 90%–20% solvent D; 40–100 min, 20% solvent D. Multiple fractions were collected, followed by validation using analytical Innoval C-18 column (250 × 4.6 mm, 5 μm, Angela tech, China). This process was repeated 25 times, and the collected fractions were merged and dried. The dried sample prepared from rotary evaporation was again injected into the preparative dynamic axial compression column and eluted with 100% solvent D for 10 min and 20% solvent D for 15 min, resulting in a solution of dopaxanthin. The acetonitrile and acetic acid were then removed through rotary evaporation, followed by freeze-drying to obtain authentic dopaxanthin. The dopaxanthin content was quantified by linear fitting of concentration and LC peak area. The calibration curve equation is $Y = 49{,}501 \times X + 19.84$ at wavelengths of 471 nm, while Y represents LC peak area and X represents dopaxanthin concentration (g/L) (Fig. S1).

## Results

#### Screening high-performance dioxygenase

DODA was the first critical enzyme for dopaxanthin synthesis. To mine the efficient DODA enzymes for dopaxanthin production, 25 DODA enzymes (Table S4) were selected based on the criterion that the amino acid identity of target sequences exceeded 45% when compared with reported enzyme AET43288.1 (DODA from *Beta vulgaris*) [22], WP_012222467.1 (DODA from *Gluconacetobacter diazotrophicus*) [23] and QGV12702.1 (DODA from *Amanita muscaria*) [24] for test. It could be seen that these 25 enzymes were divided into two clades. The upper clade was composed of *Agaricales*, bacterial, and alga-originated DODAs, and the lower clade was composed of *Caryophyllales*, silkworm, and *E. coli*-originated DODAs (Fig. 2a).

When the recombinant plasmids harboring the DODA enzymes (Table S2) were introduced into *E. coli* (Table S1), 20 recombinant enzymes exhibited various levels of DOPA-4, 5-dioxygenase activity except KAF9464553.1, KAF8352199.1, WP 000188362.1, CAE45178.1, and BAH66636.1 (Fig. 2a). Most of recombinant DODA enzymes facilitated dopaxanthin production with the increase of catalytic time, temperature and whole-cell concentration at pH 6.0 except

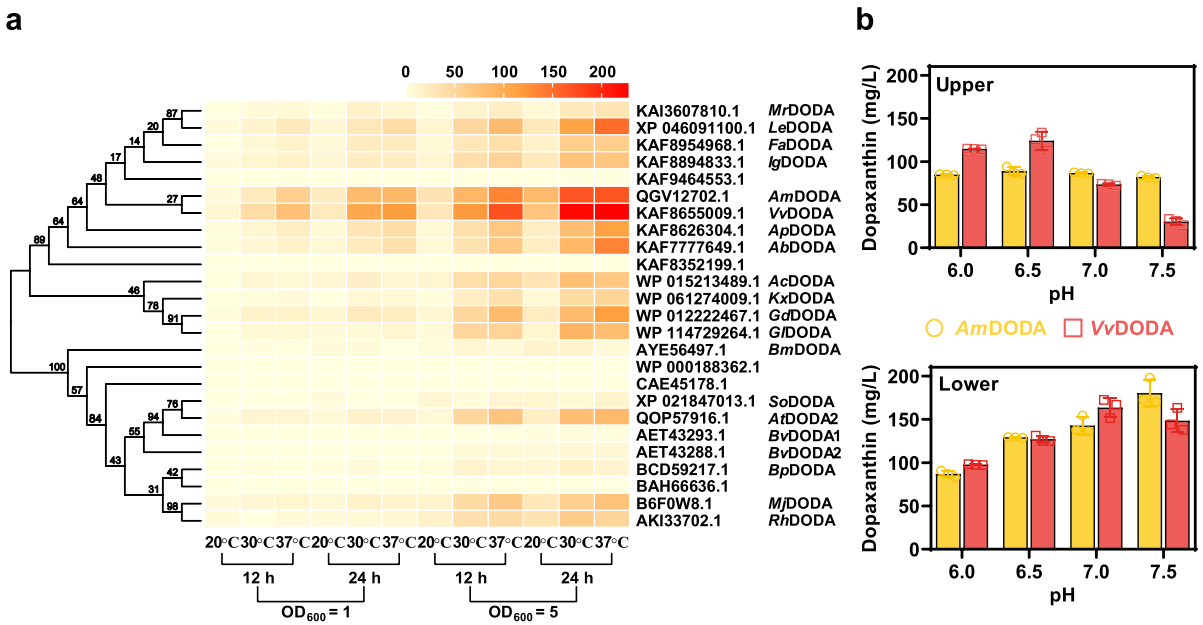


**Fig. 2** DODAs mining through phylogenetic analysis and whole-cell catalysis. **a** Screening of high-performance DODA through phylogenetic analysis and whole-cell catalysis at varied temperatures, catalytic time, and biomass. **b** Comparison of the titer of dopaxanthin synthesized by *Am*DODA and *Vv*DODA through whole-cell catalysis under different conditions. Data with error bars represent the means and standard deviations

*Ac*DODA, *Bm*DODA and *Bp*DODA, and these three enzymes showed higher activity at 30 ℃ other than 37 ℃ (Fig. 2a). Among the 25 enzymes, *Am*DODA and *Vv*DODA presented the higher catalytic activity, yielding 84.86 and 114.61 mg/L of dopaxanthin, respectively, when the catalytic temperature was 37 ℃ and whole-cell concentration was 1.0 $OD_{600}$ (Fig. 2a). The production of dopaxanthin further increased to 166.81 and 227.47 mg/L when 5.0 $OD_{600}$ whole-cell was used (Fig. 2a).

Next, the activities of *Am*DODA and *Vv*DODA were characterized under different pH conditions. The activity of *Am*DODA varied slightly from pH 6.0 to 7.5. It could synthesize up to 88.89 mg/L of dopaxanthin at pH 6.5 in the presence of 1.0 $OD_{600}$ whole-cell (Fig. 2b, the upper part). However, the activity of *Vv*DODA varied greatly from pH 6.0 to 7.5, with the highest titer 124.06 mg/L dopaxanthin at pH 6.5 in presence of 1.0 $OD_{600}$ whole-cell (Fig. 2b, the upper part). After supplementing 1.0 mM vitamin C, the titer of dopaxanthin increased significantly as vitamin C acted as an antioxidant to prevent the oxidation of L-DOPA and betalamic acid. The *Am*DODA-catalyzed titer of dopaxanthin rose from 88.89 to 180.25 mg/L, while the *Vv*DODA-catalyzed titer of dopaxanthin rose from 124.06 to 163.85 mg/L (Fig. 2b, the lower part).

## Engineering de novo dopaxanthin production in 3-dehydroshikimate hyperproducing *E. coli*

In our previous report, a 3-dehydroshikimate (DHS) hyperproducing *E. coli* WJ060 (Table S1) that could produce 90 g/L 3-dehydroshikimate (DHS) with a total yield of 33.0% mol/mol glucose was developed [18]. To channel DHS to L-DOPA, the critical precursor of dopaxanthin, shikimate dehydrogenase (AroE) was overexpressed by inserting high-expression-level synthetic part $P_{M1\text{-}93}$ [19] upstream of *aroE* in *E. coli* WJ060, resulting in a strain T001. Flask fermentation results indicated that T001 synthesized 0.7 g/L L-tyrosine without any DHS accumulation (Fig. 3a) after 36 h cultivation. Then, the replacement of wild-type chorismate mutase/prephenate dehydrogenase TyrA with $P_{M1\text{-}93}$-driven feedback-relieved version $TyrA^{M53I/A354V}$ (resulting in the strain T002) further enhanced L-tyrosine titer to 2.62 g/L (Fig. 3a).

Biosynthesis of dopaxanthin began with the hydroxylation of L-tyrosine into L-DOPA by 4-hydroxyphenylacetate 3-hydroxylase HpaBC (Fig. 1). Normally, the expression of *hpaBC* operon was deficient in *E. coli*. The expression level of *hpaB* and *hpaC* in strain T003 achieved by inserting regulatory part $P_{M1\text{-}93}$ upstream of the *hpa* operon, was improved 13.97 and 11.10 times (Fig. S2). As a result, almost all L-tyrosine was hydroxylated by HpaBC, achieving up to 3.36 g/L L-DOPA at 48 h

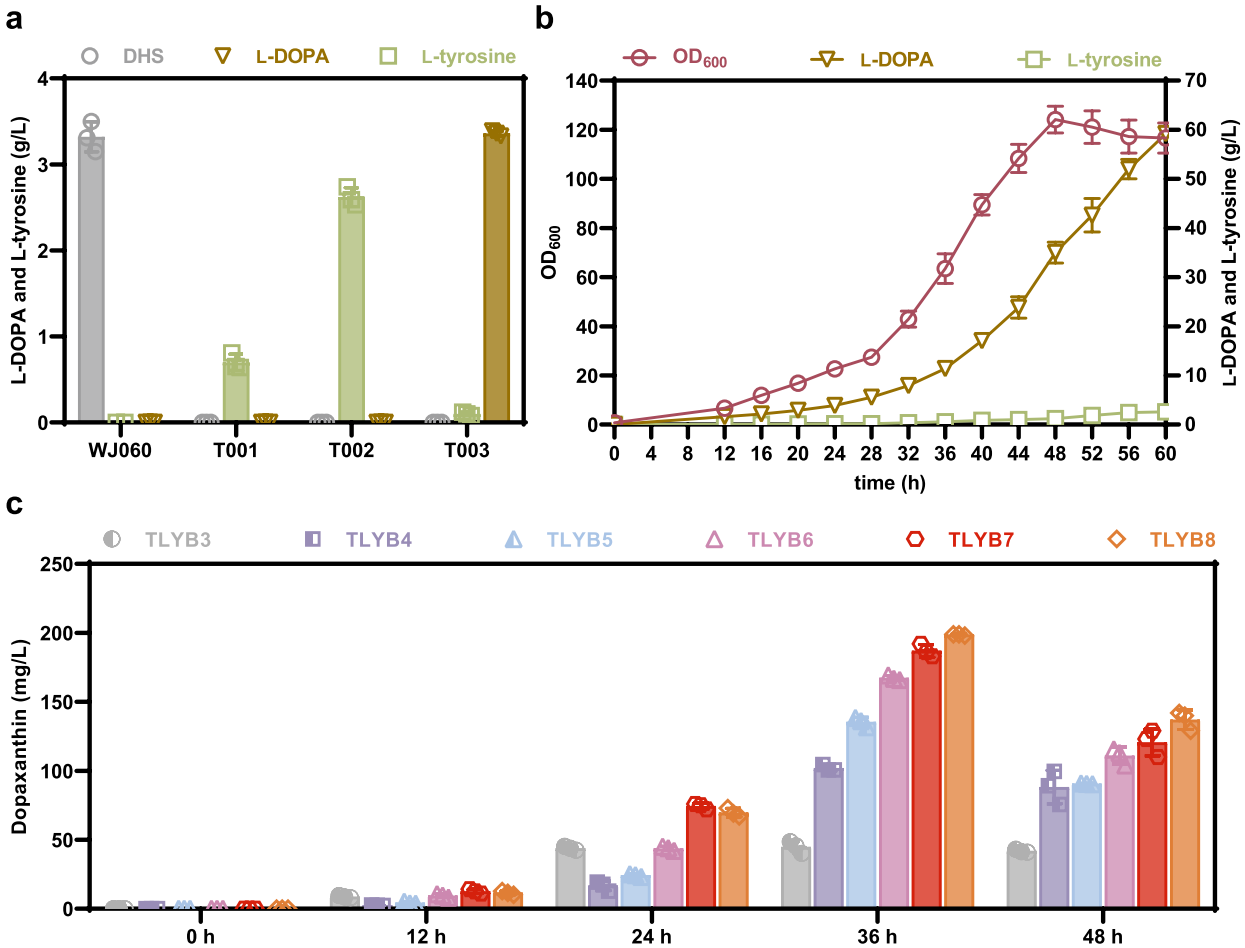


**Fig. 3** Engineering de novo dopaxanthin production from DHS-hyperproducing strain. **a** Flask fermentation of Strain WJ060, T001, T002 and T003. **b** Scale-up fermentation of T003 for L-DOPA production. **c** Flask fermentation of dopaxanthin-producing strains. Data with error bars represent the means and standard deviations

(Fig. 3a). Then, scale-up fermentation was conducted. The results indicated that T003 could synthesize up to 60.0 g/L L-DOPA after 60 h with 16.8% mol L-DOPA per mol glucose (Fig. 3b). *hpaD* in *E. coli* encodes 3,4-dihydroxyphenylacetate 2,3-dioxygenase, which catalyzes the formation of 5-carboxymethyl-2-hydroxybenzoic semialdehyde (CHMS) from L-DOPA [25]. To avoid the degradation of L-DOPA, the *hpaD* gene was deleted. Deletion of *hpaD* did not significantly increase the L-DOPA titer (Fig. S3). This may be caused by the fact that this gene is usually repressed by regulator HpaR and induced by aromatic compound as the sole carbon source [25].

To construct a strain for de novo synthesis of dopaxanthin, YgiD that possessed 4,5-DOPA dioxygenase activity [26] was firstly overexpressed with regulatory part $P_{M1\text{-}93}$. Flask fermentation results indicated that no dopaxanthin was synthesized by YgiD-overexpressed strain TLYB2. Thereby, cassettes $P_{M1\text{-}93}$-*Am*DODA and $P_{M1\text{-}93}$-*Vv*DODA were inserted into the *ygiD* site of TLYB1, respectively, to obtain strain TLYB3 and TLYB4 (Table S1). As the fermentation time prolonged, the color of the fermentation broth gradually changed from colorless to yellow and finally to red. Quantitative analysis with HPLC showed that TLYB3 and TLYB4 produced 2.41 and 2.02 g/L L-DOPA, which is lower than that of T003 (Figs. S3 and 3a). However, two new peaks at 7.2 and 11.6 min at wavelengths of 471 and 414 nm (Fig. S4a–f) were presented in the HPLC spectrum. Accurate mass of MS and fragmentation spectra of $MS^2$ ions indicated that peaks at 7.2 min were dopaxanthin (Fig. S4d, e) and peaks at 11.6 min were betalamic acid (Fig. S5g, h), which were consistent with previous reports [24, 27]. Based on the equation of the calibration curve (Fig. S1), 44.75 and 101.96 mg/L dopaxanthin were synthesized after 36 h flask fermentation by TLYB3 and TLYB4, respectively (Fig. 3c). The higher titer of dopaxanthin produced by TLYB4 when compared with TLYB3 indicated that *Vv*DODA was more suitable for de novo synthesis.

Overall, de novo synthesis of dopaxanthin is feasible by connecting the blocked pathway from DHS to L-DOPA and introducing appropriate dioxygenase.

#### Increasing dopaxanthin production with evolved *Vv*DODA

A large amount of precursor L-DOPA and less product dopaxanthin in the endpoint fermentation broth (Figs. 3 and S3) indicated insufficient activity of *Vv*DODA. To improve *Vv*DODA activity, a high-throughput screening method (Fig. S6), including the creation of a mutant library by error-prone PCR that transformed into L-DOPA-producing strain TLYB1, and screening based on the optical absorption property of dopaxanthin at λmax = 471 nm was carried out.

In the first round of screening, a mutant 39F6 with enhanced activity won out of 9600 mutants. Sequencing analysis revealed that there were two missense mutations and one synonymous mutation in *Vv*DODA: D68V, a mutation from codon GAU to GUU, I103V, a mutation from codon AUU to GUU, and L104, a mutation from codon CUG to CUA. To investigate the impact of each missense mutation on the titer of dopaxanthin, the single point mutation strain TLYB1-26-D68V and TLYB1-26-I103V that containing *Vv*DODA$^{D68V}$ and *Vv*DODA$^{I103V}$, respectively, were developed (Table S1). The titer of dopaxanthin produced by strain 39F6, TLYB1-26-D68V, and TLYB1-26-I103V is 78.37, 54.15 and 90.01 mg/L, respectively, which was 11.64% higher, 29.64% lower, 28.2% higher than that of control strain TLYB1-26 (the strain TLYB1with pTLY26) (Fig. S7). These results indicated that the I103V mutation is beneficial to the biosynthesis of dopaxanthin, whereas the D68V mutation is harmful.

To further investigate the impact of these two sites on dopaxanthin biosynthesis, saturation mutations on D68 and I103 were performed. It was found that the majority of strains carrying mutation at position 103 were unable to synthesize dopaxanthin except for the strains with *Vv*DODA$^{I103L}$, *Vv*DODA$^{I103C}$, or *Vv*DODA$^{I103V}$ (Fig. S7). Among them, the titer of dopaxanthin synthesized by strain with *Vv*DODA$^{I103L}$ and *Vv*DODA$^{I103C}$ decreased by 8.5 and 29.47%, while the strain with *Vv*DODA$^{I103V}$ increased by 18.62% when compared to that of the control group (Fig. S7). The saturation mutation at D68 weakened the dopaxanthin-producing capacity of all strains, particularly D68P (Fig. S7).

Next, the second round of screening was carried out to further improve enzyme activity based on the mutant *Vv*DODA$^{I103V}$, and a new strain named 47D4 with further enhanced titer won out of another 4800 mutants, which could produce 98.4 mg/L dopaxanthin after 36 h fermentation (Fig. S7). Sequencing analysis showed that the codon of the 114th amino acid mutated from CGT to GCG, resulting in a transition from arginine residue (R) to alanine residue (A).

Compared to that of plasmid expression, the higher titer of dopaxanthin was achieved by genomic expression of *Vv*DODA (strain TLYB4 in Fig. 3c vs. TLYB1-26 in Fig. S7). Thus, the *ygiD* locus of TLYB1 was replaced with cassettes $P_{M1-93}$-*Vv*DODA$^{I103V}$ and $P_{M1-93}$-*Vv*DODA$^{I103V/R114A}$, resulting in the strains TLYB5 and TLYB6 (Table S1). The titer of dopaxanthin increased to 135.43 and 167.30 mg/L by TLYB5 and TLYB6, which were 32.83% and 64.08% higher than that of TLYB4, respectively (Fig. 3c). The titers of L-DOPA, 1.69 and 1.40 g/L, produced by TLYB5 and TLYB6 were lower than that of TLYB4 (Fig. S3). This result manifested that the performance of the strain TLYB6 with *Vv*DODA$^{I103V/R114A}$ significantly exceeded that of WT vision.

The overexpression of recombinant protein confirmed that *Vv*DODA and its mutants, *Vv*DODA$^{I103V}$ and *Vv*DODA$^{I103V/R114A}$, all could be solubly expressed at a similar level in *E. coli* (Fig. 4a). As shown in Fig. 4b, the optimal pH for these recombinant enzymes was 7.0, and within the range of pH 6.5–7.5, more than 50% of their activity was preserved. The optimal temperature for wild-type *Vv*DODA is 45 ℃. On the contrary, the optimal temperature for *Vv*DODA$^{I103V}$ and *Vv*DODA$^{I103V/R114A}$ increased by ten degrees to 55 ℃ (Fig. 4c). The kinetic parameter test of the three recombinant enzymes showed that compared with the wild-type, the substrate affinity of *Vv*DODA$^{I103V}$ and *Vv*DODA$^{I103V/R114A}$ increased by 1.84 times and 5.37 times. The catalytic number increased by 2.26 times and 6.33 times, resulting in a 4.16 and 34 times increase in catalytic efficiency, respectively (Fig. 4d and Table 1).

To further probe the effect of mutations on the catalytic efficiency of *Vv*DODA, the structures of *Vv*DODA and its mutants were modeled by AlphaFold3 (Fig. 5) [28]. Catalytic pockets were predicted by PrankWeb, a machine learning-based method for the prediction of ligand binding sites from protein structure. According to the prediction results, *Vv*DODA, *Vv*DODA$^{I103V}$ and *Vv*DODA$^{I103V/R114A}$ might have three, two, and two catalytic pockets, respectively. Based on the size of catalytic pocket whether large enough to accommodate L-DOPA, metal ions, and oxygen, pocket I of the three enzymes should be the site where the reaction occurred. The volume of pocket I of *Vv*DODA was 793.4 Å$^3$, which was comprised of amino acid residues H25, H27, R64, N66, I70, G71, P72, H73, E79, H106, E112, H116, T133, L134, P142, Q144 (Fig. 5a). However, the volume of pocket I of *Vv*DODA$^{I103V}$ and *Vv*DODA$^{I103V/R114A}$ decreased to 753.9 and 691.2 Å$^3$, respectively, due to the alteration of a few amino acids involved in pocket composition (Fig. 5b, c). Furthermore, the longitudinal distance of pocket I

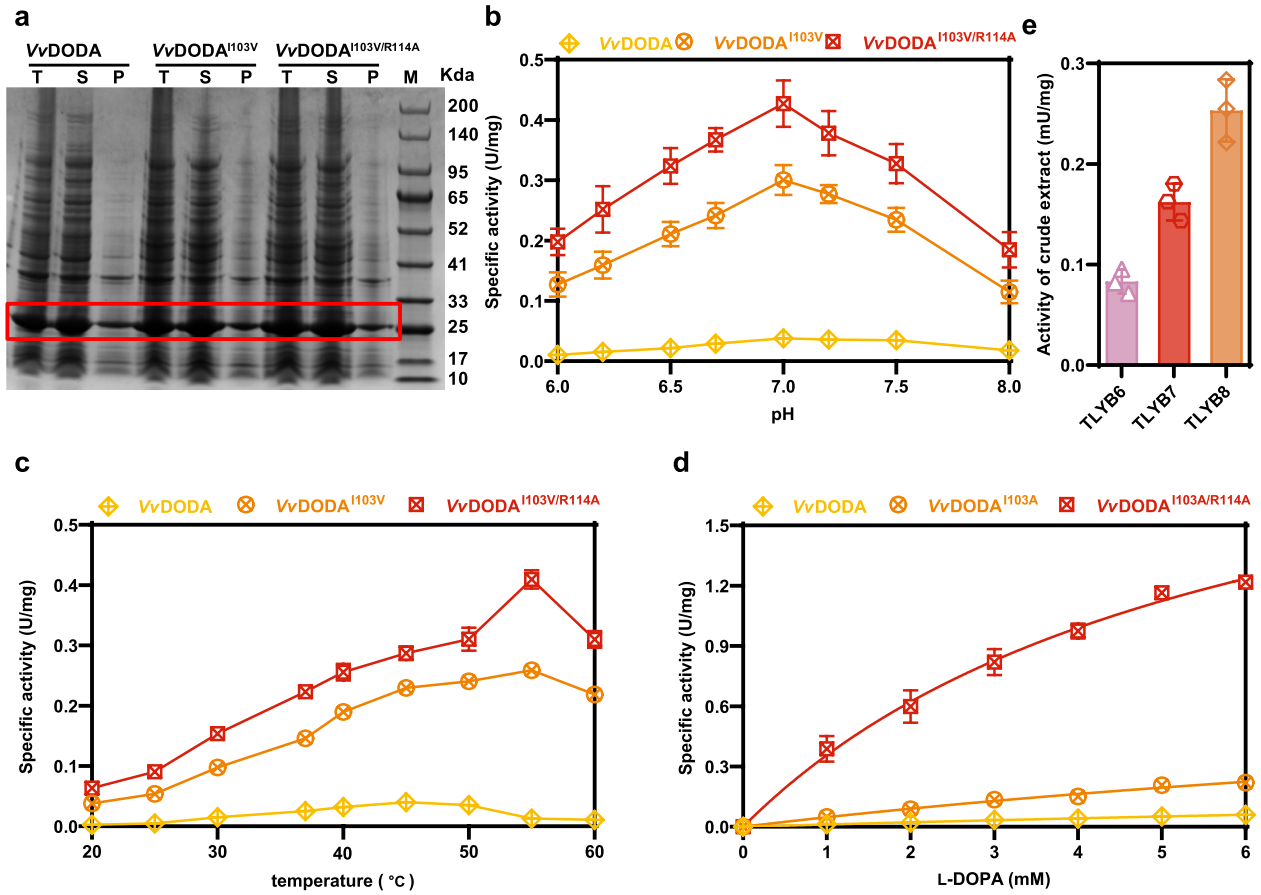


**Fig. 4** Electrophoresis and Enzyme activity analysis of *Vv*DODA, *Vv*DODA$^{I103V}$, and *Vv*DODA$^{I103V/R114A}$. **a** Electrophoresis analysis of *Vv*DODA, *Vv*DODA$^{I103V}$, and *Vv*DODA$^{I103V/R114A}$. T represents the total disruption fraction, S represents the supernatant, and P represents the precipitation. **b**–**d** Effect of pH, temperature, and L-DOPA concentration on the specific activity of *Vv*DODA, *Vv*DODA$^{I103V}$, and *Vv*DODA$^{I103V/R114A}$. Data with error bars represent the means and standard deviations. **e** Crude enzyme activity analysis of the supernatant of disrupted TLYB6, TLYB7, and TLYB8

**Table 1** Parameters of dioxygenase

| Enzyme | Km (mM) | Kcat ($min^{-1}$) | Kcat/Km ($mM^{-1}·min^{-1}$) | Optimum pH | Optimum temperature (℃) | Inducing temperature (℃) | References |
|---|---|---|---|---|---|---|---|
| *Vv*DODA | 31.83[a] | 0.3845[a] | $1.208\times10^{-2}$ | 7.0 | 45 | 30 | This work |
| *Vv*DODA$^{I103V}$ | 17.30[a] | 0.87[a] | $5.029\times10^{-2}$ | 7.0 | 55 | 30 | This work |
| *Vv*DODA$^{I103V/R114A}$ | 5.931[a] | 2.435[a] | $4.106\times10^{-1}$ | 7.0 | 55 | 30 | This work |
| *Bv*DODA | 6.9 | 0.095 | $1.377\times10^{-2}$ | 8.5 | 25[b] | 20 | [22] |
| *Ec*YgiD | 7.9 | 0.17 | $2.152\times10^{-2}$ | 8.5 | 25[b] | 20 | [26] |
| *Am*DODA | 4.2 | 54.6 | 13 | 8.5 | 25[b] | 30 | [24] |
| *Gd*DODA | 1.36 | 0.50 | $3.676\times10^{-1}$ | 6.5 | 25[b] | 20 | [23] |
| *Bm*DODA | 1.06 | – | – | 8.5 | 30 | 16 | [30] |
| *Ac*DODA | 53 | – | – | 7.0 | 25[b] | 20 | [29] |

[a] The parameters of catalytic activity were obtained at 37 ℃

[b] Effect of temperature on DODA was only tested at 25 ℃

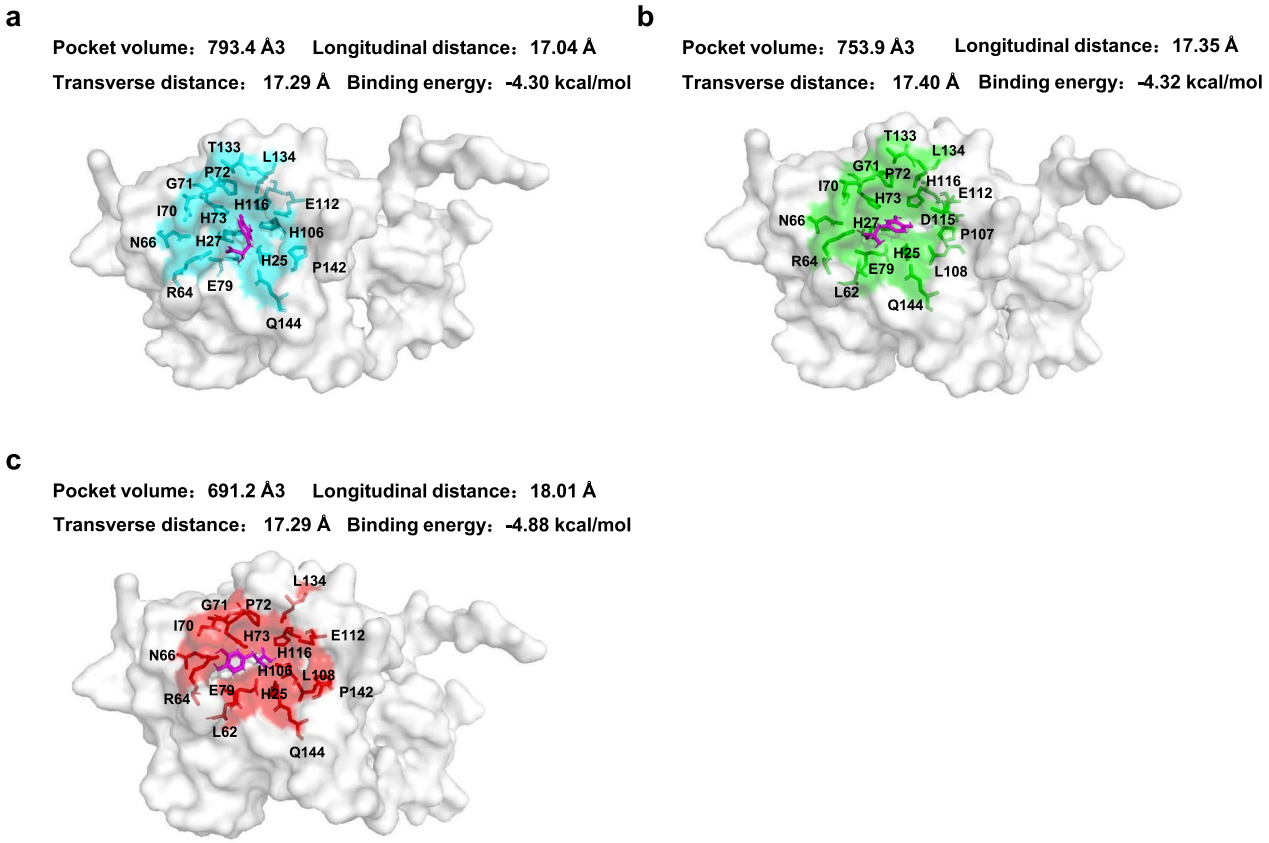


**Fig. 5** Catalytic pockets predicted by PrankWeb based on structures modeled by AlphaFold3. **a** *Vv*DODA, **b** *Vv*DODA$^{I103V}$ and **c** *Vv*DODA$^{I103V/R114A}$

opening in *Vv*DODA$^{I103V}$ increased and the transverse distance decreased slightly (Fig. 5; Tables S5 and S6). As for *Vv*DODA$^{I103V/R114A}$, the transverse and longitudinal distances of pocket I opening were both enlarged when compared with that of *Vv*DODA (Fig. 5, Table S5 and S7). The mutation of I103V resulted in the lower left movement of lid composed of R64 and N66 while the mutation of R114A brought the right edge of the opening to move outward (Fig. 5). The increase of catalytic opening was beneficial for the entry of substrates while the reduction of catalytic pockets may enhance the affinity between proteins and substrates.

Based on the above results, the elevated titer of dopaxanthin was triggered by two missense mutations that dramatically enhanced DODA performance.

### Optimizing biosynthetic pathway enabling efficient production of dopaxanthin

Upon increasing the dioxygenase performance to enable the highest reported titer of dopaxanthin with flask fermentation, fed-batch fermentations were performed in a synthetic medium with glucose as the carbon source. The results showed that the productivity of dopaxanthin was low in the first 20 h but accelerated after 20 h (Fig. 6). The stepwise increase of dopaxanthin leads to a change in the color of the fermentation broth from brown to reddish black (insets in Fig. 6). The strain TLYB6 with mutant *Vv*DODA$^{I103V/R114A}$ could produce 21.31 g/L dopaxanthin, which was 573% higher than the 3.72 g/L dopaxanthin produced by the strain TLYB4 with wild-type *Vv*DODA. Nevertheless, there was still a large amount of L-DOPA in the fermentation broth. The titer of by-product L-DOPA reached 24.62 and 19.19 g/L for the strain TLYB4 and TLYB6, respectively (Fig. 6b, c). To reduce the accumulation of L-DOPA and increase the titer of dopaxanthin, the second and third copy of cassette $P_{M1\text{-}93}$-*Vv*DODA$^{I103V/R114A}$ was inserted into the *ldhA* and *pflB* locus of TLYB6, respectively, resulting in strain TLYB7 and TLYB8 with multiple copies of *Vv*DODA$^{I103V/R114A}$ (Fig. 6a and Table S1).

The expression level *Vv*DODA$^{I103V/R114A}$ in the strain TLYB7 with two copies and TLYB8 with three copies, semi-quantified by qRT-PCR analysis, was improved by 2.00 and 2.83 times compared with that of the strain TLYB6 with only one copy (Fig. S2c). The results of crude enzyme activity determination were also similar

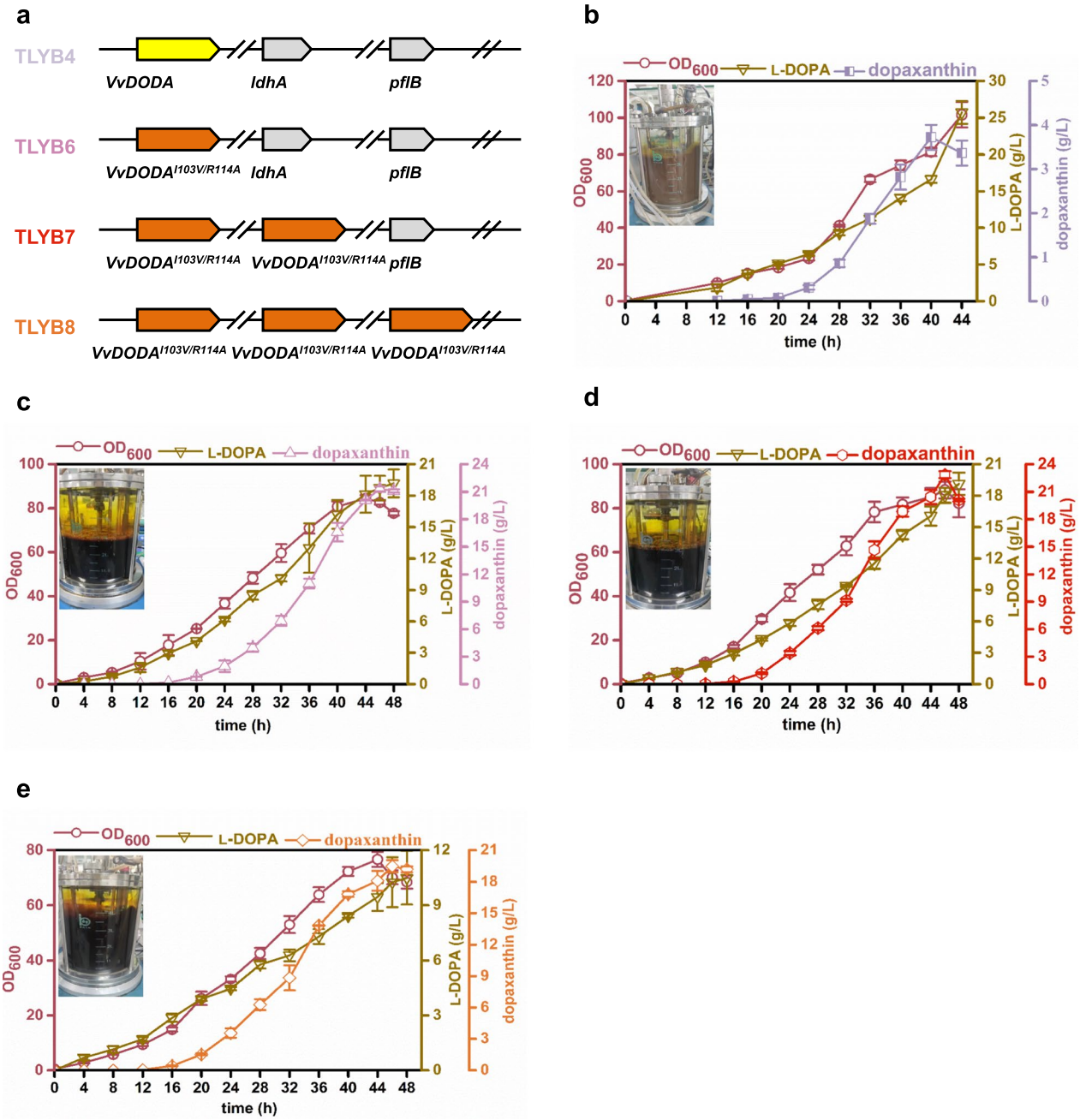


**Fig. 6** Scale-up fermentation of TLYB4, TLYB6, TLYB7 and TLYB8. **a** Characteristics of the synthetic pathway of dopaxanthin. **b** Scale-up fermentation of TLYB4. **c** Scale-up fermentation of TLYB6. **d** Scale-up fermentation of TLYB7. **e** Scale-up fermentation of TLYB8. Data with error bars represent the means and standard deviations

(Fig. 4e). The increase in expression level led to a rise in yield. 187.0 and 198.7 mg/L dopaxanthin was produced by the strain TLYB7 and TLYB8 after 36 h in flask fermentation, which was 11.98% and 18.98% higher than that of TLYB6 (Fig. 3c). Scale-up fermentation indicated that strain TLYB7 produced higher levels of dopaxanthin within 46 h of fermentation, achieving up to 22.87 g/L. However, the titer of dopaxanthin produced by strain TLYB8, 19.50 g/L, was slightly lower than that of TLYB6 and TLYB7 within 46 h. This may be attributed to the metabolic burden brought by multi-copy expression.

## Discussions and conclusions

DODAs were found in fungi, bacteria, insects, and plants, such as *Amanita muscaria* [24], *E. coli* [26], *Gluconacetobacter diazotrophicus* [23], *Anabaena cylindrical* [29], *Bombyx mori* [30], *Beta vulgaris* L [22], *Amaranthus tricolor* [31] etc., some of which were employed for heterologous biosynthesis of betalains. However, the reported titer was relatively low, mainly due to the low performance of DODA and the low content of critical precursor L-DOPA.

In our study, homologous sequence alignment followed by whole-cell catalysis and de novo synthesis strategy was employed to mine novel dioxygenases from the database, with the titer of dopaxanthin as the indicator. This means that the high titer of dopaxanthin is inevitably due to the superior performance of the DODA. An efficient dioxygenase derived from *Volvariella volvacea* WC 439 won out of 25 DODAs (Figs. 2 and 3c). 114.61 mg/L titer of dopaxanthin was produced through whole-cell catalysis, which was higher than that synthesized using *Mj*DODA or *Gd*DODA [15, 16].

Starting from the DHS-hyperproducing strain WJ060, strain T003, featured with the capability to produce the highest titer of L-DOPA, was conceived by strengthening the critical redox enzyme AroE [32], relieving the feedback inhibition of crucial enzymes TyrA by L-tyrosine, and activating the silenced gene cluster *hpabc*. Benetifited by the high precursor concentration (60 g/L) and high performance of evolved DODA, 101.96 mg/L and 3.72 g/L dopaxanthin were synthesized by strain TLYB4 at the flask and scale-up fermentation levels. This titer achieved by flask fermentation is 1.28 times that of the highest bioreactor level of 79.96 mg/L achieved by adding the precursor L-DOPA [16]. Compared at the scale-up fermentation level, the titer of dopaxanthin synthesized by the TLYB4 strain reported in this study was 46.52 times higher than previous report [16].

Directed evolution further enhances the performance of dioxygenases, boosting substrate affinity by 5.37 times, catalytic efficiency by 34 times, and optimal catalytic temperature by 10 ℃ (Fig. 4 and Table 1). Although partial kinetic parameters of *Gd*DODA and *Am*DODA were better than or comparable to those of *Vv*DODA$^{I103V/R114A}$, the titer of dopaxanthin produced by *Gd*DODA and *Am*DODA-harboring strains was lower than that of *Vv*DODA$^{I103V/R114A}$, both in this study (Figs. 2 and 3c) or in other reports [16, 24]. This was caused by higher protein expression level, more suitable optimum catalytic pH value, and enhanced thermal stability of *Vv*DODA$^{I103V/R114A}$ (Fig. 4 and Table 1). The optimal catalytic temperature of *Vv*DODA$^{I103V/R114A}$ reached 55 ℃, much higher than that of other reported enzymes (Fig. 4b and Table 1). Its optimal catalytic pH value was 7.0, closer to the intracellular pH of *E. coli* than that of *Am*DODA at 8.5 (Fig. 4c and Table 1) [33]. Additionally, the protein expression of *Vv*DODA$^{I103V/R114A}$ was more robust, as evidenced by the induced temperature being elevated at 30 ℃, which was higher than other reported 25 ℃ or lower (Table 1).

All mutations of I103 residue lose activity, except for mutations I103L, I103V, and I103C. This may be caused by the shortening of amino acid side chains. Of course, further shortening of amino acid side chains could also inactive enzymes, such as I103A and I103G. In addition to changes in side chain volume, changes in hydrophobicity may also reduce/inactivate enzyme activity, such as I103C, I103S, I103T and I103N. All mutations of D68 residue remain active, except for D68P. This may be due to the D68 residue being far from the conserved amino acid residue H106 [34].

The mutation of I103V resulted in the lower left movement of lid composed of R64 and N66, enlarging the longitudinal distance of pocket I opening, while the mutation of R114A brought the right edge of the opening to move outward (Fig. 5). The mutations of I103V and R114A also led to a decrease in binding energy, from −4.30 kcal/mol between WT and substrate to −4.32 kcal/mol between *Vv*DODA$^{I103V}$ and substrate, and −4.88 kcal/mol between *Vv*DODA$^{I103V/R114A}$ and substrate (Fig. 5). At the same time, the number of hydrogen bonds formed between substrate and enzyme also changed, increasing from 6 between WT and substrate to 9 between *Vv*DODA$^{I103V/R114A}$ and substrate. As a result, the enhancement of enzyme performance, including enhancement in substrate affinity and catalytic efficiency, could be explained by the variation of the catalytic pocket, binding energy and hydrogen bond number (Fig. 5, Tables S5, S6, S7 and S8).

Given these advantages, the dopaxanthin titer increased to 167.3 mg/L through *Vv*DODA$^{I103V/R114A}$ containing strain TLYB6. At the scale-up fermentation level, dopaxanthin increased from 3.72 to 21.31 g/L, reaching a 5.73-fold and 267-fold increase when compared to TLYB4 and previous report [16]. These results conclude that a high-performance DODA conceived through protein engineering significantly elevates the dopaxanthin-produce phenotype. It also confirms that high precursor promotes the synthesis of dopaxanthin.

Natural pigments own significant health and environmental advantages compared to chemically synthesized pigments. However, the acquisition of natural pigments heavily relies on plant extraction. While plant cultivation is land and resource-demanding, fermentation-based processes employing genetically modified microorganisms are feasible alternative natural pigment sources. To this end, we extended the DHS-hyperproducing strain to

synthesize yellow dopaxanthin via fermentation at dozens of gram-scale in a bioreactor—resulting in 22.87 g/L, a 286-fold improvement compared with previous attempts [16]. The unprecedented high titer of dopaxanthin, achieved by addressing the rate-limiting enzyme and the high concentration of precursor L-DOPA, significantly reduced the cost of the fermentation and downstream steps. It is roughly estimated that the cost of dopaxanthin could be as low as 150 RMB/kg according to the assumption that costs are distributed equally between upstream and downstream [35]. This pure dopaxanthin cost is comparable to or below the price of E162 (0.4–1.2% betalain content) made from engineered *Yarrowia lipolytica* or beetroot [35].

It was revealed that the impacts of the traditional betanin extraction process are approximately five times higher for human health and three times higher for both ecosystem quality and resources compared with the impacts of fermentation [35]. According to this result, we also roughly infer that the fermentation-based dopaxanthin production possesses a superior environmental sustainability performance compared with the extraction-based process based on two criteria: higher titer increases environmental performance [35] and higher fermentation temperature reduces cooling water consumption [36], as the titer of dopaxanthin in this study is much higher than that of betanin in *Y. lipolytica*, and the fermentation temperature is much higher (37 vs. 30 ℃).

This work not only aimed to produce economically viability dopaxanthin by developing an efficient microbial factory as a controllable system but also presents an opportunity to expand our work to the biomanufacturing of other plant betalains that currently are not commercially available owing to their low native content in the respective plants.

## Supplementary Information

The online version contains supplementary material available at https://doi.org/10.1186/s12934-024-02597-6.

Additional file1.

### Author contributions

QW and XJ conceived the topic and designed the study. LT, WC, and XJ performed all of the experiments. XJ and LT wrote the manuscript. QW modified the manuscript.

### Funding

This work was supported by the National Natural Science Foundation of China (No. 32200063), the National Key Research and Development Program of China (No. 2021YFC2103300), the Key Research and Development Program of Hebei Province (No. 23372801D), Natural Science Foundation of Hebei Province (No. C2023106028) and the China Postdoctoral Science Foundation (No. 2022M723339).

### Data availability

No datasets were generated or analysed during the current study.

## Declarations

### Ethics approval and consent to participate

This article does not contain any studies with human participants or animals performed.

### Competing interests

The authors declare no competing interests.

Received: 21 September 2024 Accepted: 19 November 2024
Published online: 18 December 2024

### References

1. Martins N, Roriz CL, Morales P, Barros L, Ferreira IC. Food colorants: challenges, opportunities and current desires of agro-industries to ensure consumer expectations and regulatory practices. Trends Food Sci Technol. 2016;52:1–15.
2. Grotewold E. The genetics and biochemistry of floral pigments. Annu Rev Plant Biol. 2006;57:761–80.
3. Miguel MG. Betalains in some species of the *Amaranthaceae* family: a review. Antioxidants (Basel). 2018;7:53.
4. European Food Safety Authority. Scientific Opinion on the re-evaluation of beetroot red (E 162) as a food additive. EFSA J. 2015;13:4318.
5. 21CFR73.40 Dehydrated beets (beet powder) [https://www.accessdata.fda.gov/scripts/cdrh/cfdocs/cfCFR/CFRSearch.cfm?CFRPart=73]
6. Gandia-Herrero F, Escribano J, Garcia-Carmona F. The role of phenolic hydroxy groups in the free radical scavenging activity of betalains. J Nat Prod. 2009;72:1142–6.
7. Gliszczyńska-Świgło A, Szymusiak H, Malinowska P. Betanin, the main pigment of red beet: molecular origin of its exceptionally high free radical-scavenging activity. Food Addit Contam. 2006;23:1079–87.
8. Harris NN, Javellana J, Davies KM, Lewis DH, Jameson PE, Deroles SC, Calcott KE, Gould KS, Schwinn KE. Betalain production is possible in anthocyanin-producing plant species given the presence of DOPA-dioxygenase and L-DOPA. BMC Plant Biol. 2012;12:34.
9. Gandía-Herrero F, Cabanes J, Escribano J, García-Carmona F, Jiménez-Atiénzar M. Encapsulation of the most potent antioxidant betalains in edible matrixes as powders of different colors. J Agric Food Chem. 2013;61:4294–302.
10. Guadarrama-Flores B, Rodríguez-Monroy M, Cruz-Sosa F, Garcia-Carmona F, Gandia-Herrero F. Production of dihydroxylated betalains and dopamine in cell suspension cultures of Celosia argentea var. plumosa. J Agric Food Chem. 2015;63:2741–9.
11. Tanaka Y, Sasaki N, Ohmiya A. Biosynthesis of plant pigments: anthocyanins, betalains and carotenoids. Plant J. 2008;54:733–49.
12. Impellizzeri G, Piattelli M, Sciuto S. A new betaxanthin from *Glottiphyllum longum*. Phytochem. 1973;12:2293–4.
13. Spórna-Kucab A, Tekieli A, Grzegorczyk A, Świątek Ł, Rajtar B, Skalicka-Woźniak K, Starzak K, Nemzer B, Pietrzkowski Z, Wybraniec S. Metabolite profiling analysis and the correlation with biological activity of betalain-rich *Portulaca grandiflora* Hook Extracts. Antioxidants (Basel). 2022;11:1654.
14. Tsien RY. The green fluorescent protein. Annu Rev Biochem. 1998;67:509–44.
15. Hou Y, Liu X, Li S, Zhang X, Yu S, Zhao G-R. Metabolic engineering of *Escherichia coli* for *de novo* production of betaxanthins. J Agric Food Chem. 2020;68:8370–80.
16. Guerrero-Rubio MA, López-Llorca R, Henarejos-Escudero P, García-Carmona F, Gandía-Herrero F. Scaled-up biotechnological production of individual betalains in a microbial system. Microb Biotechnol. 2019;12:993–1002.
17. Babaei M, Thomsen PT, Dyekjær JD, Glitz CU, Pastor MC, Gockel P, Körner JD, Rago D, Borodina I. Combinatorial engineering of betalain biosynthesis pathway in yeast *Saccharomyces cerevisiae*. Biotechnol Biofuels Bioprod. 2023;16:128.

18. Wang X, Wu F, Zhou D, Song G, Chen W, Zhang C, Wang Q. Cofactor self-sufficient whole-cell biocatalysts for the relay-race synthesis of shikimic acid. Ferment. 2022;8:229.
19. Lu J, Tang J, Liu Y, Zhu X, Zhang T, Zhang X. Combinatorial modulation of *galP* and *glk* gene expression for improved alternative glucose utilization. Appl Microbiol Biotechnol. 2012;93:2455–62.
20. Sharan SK, Thomason LC, Kuznetsov SG, Court DL. Recombineering: a homologous recombination-based method of genetic engineering. Nat Protoc. 2009;4:206–23.
21. Trezzini G, Zrÿb J-P. Characterization of some natural and semi-synthetic betaxanthins. Phytochem. 1991;30:1901–3.
22. Gandía-Herrero F, García-Carmona F. Characterization of recombinant *Beta vulgaris* 4, 5-DOPA-extradiol-dioxygenase active in the biosynthesis of betalains. Planta. 2012;236:91–100.
23. Contreras-Llano LE, Guerrero-Rubio MA, Lozada-Ramírez JD, García-Carmona F, Gandía-Herrero F. First betalain-producing bacteria break the exclusive presence of the pigments in the plant kingdom. MBio. 2019;10:e00345.
24. Soares DM, Gonçalves LC, Machado CO, Esteves LC, Stevani CV, Oliveira CC, Dorr FA, Pinto E, Adachi FM, Hotta CT. Reannotation of fly *Amanita* L-DOPA dioxygenase gene enables its cloning and heterologous expression. ACS Omega. 2022;7:16070–9.
25. Díaz E, Ferrández A, Prieto MA, García JL. Biodegradation of aromatic compounds by *Escherichia coli*. Microbiol Mol Biol Rev. 2001;65:523–69.
26. Gandía-Herrero F, García-Carmona F. *Escherichia coli* protein YgiD produces the structural unit of plant pigments betalains: characterization of a prokaryotic enzyme with DOPA-extradiol-dioxygenase activity. Appl Microbiol Biotechnol. 2014;98:1165–74.
27. Xie G-R, Chen H-J. Comprehensive betalain profiling of djulis (*Chenopodium formosanum*) cultivars using HPLC-Q-orbitrap high-resolution mass spectrometry. J Agric Food Chem. 2021;69:15699–715.
28. Abramson J, Adler J, Dunger J, Evans R, Green T, Pritzel A, Ronneberger O, Willmore L, Ballard AJ, Bambrick J, et al. Accurate structure prediction of biomolecular interactions with AlphaFold 3. Nature. 2024;630:493–500.
29. Guerrero-Rubio MA, García-Carmona F, Gandía-Herrero F. First description of betalains biosynthesis in an aquatic organism: characterization of 4, 5-DOPA-extradiol-dioxygenase activity in the cyanobacteria *Anabaena cylindrica*. Microb Biotechnol. 2020;13:1948–59.
30. Wang CF, Sun W, Zhang Z. Functional characterization of the horizontally transferred 4, 5-DOPA extradiol dioxygenase gene in the domestic silkworm. Bombyx mori Insect Mol Biol. 2019;28:409–19.
31. Chang Y-C, Chiu Y-C, Tsao N-W, Chou Y-L, Tan C-M, Chiang Y-H, Liao P-C, Lee Y-C, Hsieh L-C, Wang S-Y. Elucidation of the core betalain biosynthesis pathway in *Amaranthus tricolor*. Sci Rep. 2021;11:6086.
32. Li Z, Gao C, Ye C, Guo L, Liu J, Chen X, Song W, Wu J, Liu L. Systems engineering of *Escherichia coli* for high-level shikimate production. Metab Eng. 2023;75:1–11.
33. Kanjee U, Houry WA. Mechanisms of acid resistance in *Escherichia coli*. Annu Rev Microbiol. 2013;67:65–81.
34. Christinet L, Burdet FX, Zaiko M, Hinz U, Zrÿd JP. Characterization and functional identification of a novel plant 4,5-extradiol dioxygenase involved in betalain pigment biosynthesis in *Portulaca grandiflora*. Plant Physiol. 2004;134:265–74.
35. Thomsen PT, Meramo S, Ninivaggi L, Pasutto E, Babaei M, Avila-Neto PM, Pastor MC, Sabri P, Rago D, Parekh TU. Beet red food colourant can be produced more sustainably with engineered *Yarrowia lipolytica*. Nat Microbiol. 2023;8:2290–303.
36. Wang Z, Qi Q, Lin Y, Guo Y, Liu Y, Wang Q. QTL analysis reveals genomic variants linked to high-temperature fermentation performance in the industrial yeast. Biotechnol Biofuels Bioprod. 2019;12:59.


## Publisher's Note